JOURNAL OF AIRCRAFT
Vol. 50, No. 5, September–October 2013

Engineering Notes

Study on Powered-Parafoil Longitudinal Flight Performance with a Fast Estimation Model

Yang Hua,* Song Lei,† Liu Cheng,‡ and Huang Jun§
Beihang University, 100191 Beijing,
People's Republic of China

DOI: 10.2514/1.C032176

Nomenclature

C_{D_i} = induced drag coefficient
C_{D_S} = payload drag coefficient
C_{D_0} = zero-lift drag coefficient
C_L = lift coefficient
C_{M_0} = zero-lift moment coefficient
c = chord length of the airfoil, m
D = drag of the canopy, N
D_l = drag of the suspension lines, N
D_2 = drag of the payload, N
d = payload diameter, m
d_l = suspension-line diameter, m
d_T = distance of thrust line from point O, m
d_1 = length of line OF, m
F_X = resultant force on the X axis of the parafoil, N
F_Z = resultant force on the Z axis of the parafoil, N
G_1 = gravity of the canopy, N
G_2 = gravity of the payload, N
h = inlet height of the open airfoil, m
L = lift of the canopy, N
l = length of the payload, m
M = moment to the leading-edge point of the canopy, N · m
M_1 = resultant moment of the system joined by the canopy and the suspension lines, N · m
M_2 = resultant moment of the payload, N · m
m_1 = mass of the canopy, kg
m_2 = mass of the payload, kg
n = number of suspension lines
R = mean line length, m
S = canopy area, m^2
T = thrust of the motor, N
T_{cruise} = required thrust for a level flight, N
$T_{\max}$ = maximum available thrust, N
v = speed of the parafoil, m/s
$v_{z,\max}$ = maximum climbing rate, m/s
α = angle of attack of the canopy, rad
α_l = angle between the normal plane of the line and the direction of inflow, deg
γ = flight-path angle, deg
γ_{glide} = gliding angle, deg
δ = swing angle of the payload, deg

Received 24 October 2012; revision received 29 January 2013; accepted for publication 6 February 2013; published online 28 June 2013.

*Ph.D. Candidate, School of Aeronautic Science and Engineering; yhbuaa@163.com.
†Ph.D. Candidate, School of Aeronautic Science and Engineering; strikerlei@126.com.
‡Postgraduate Student, School of Aeronautic Science and Engineering; a.k.118@163.com.
§Professor, School of Aeronautic Science and Engineering; junh@china.com.

I. Introduction

PARAFOILS have more applications than traditional parachutes because of their better glide ratio and maneuverability. They are used, not only as travel carriers in sports and tourism, but also as precision aerial-delivery tools for military paratroopers and supplies. Furthermore, powered parafoils with the ability to take off from the ground and to cruise for a long time extend the possible applications.

Detailed dynamic models of parafoils have been presented in many works [1–7]. A 3-degree-of-freedom (DOF) model is precise enough for an analysis on the longitudinal plane [1,2]. A 6-DOF model treats the whole parafoil as a rigid body [3–5]. Rotations between the canopy and the payload are considered in models with greater than 6 DOF [6,7]. In addition, parametrical identification, which is based on test-flight data, is becoming an important way to achieve a good dynamic model [8,9].

The aerodynamics of a parafoil have been intensively studied using wind-tunnel tests for parafoils with different canopy shapes [10] and engineering estimation methods [11]. A computational method was also extensively used for canopy aerodynamic characteristics [12].

Studies on parafoil design methods provide engineers with direct guidance, including ways to, not only choose the configuration parameters, but also to analyze the flight performance, static stability, and inflation dynamics [13–15]. Some studies that were focused on powered parafoils discussed the many differences between powered and gliding parafoils. Ward et al.'s study of the flight performance and the configuration parameters was conducted using a complex dynamic model with more than 6 DOF [15]. It will be more wonderful that the discussion on the canopy stall, suspension-line slack, and static stability is considered in Ward et al.'s research.

A simple static model, which is more convenient for fast estimation or optimization design, was established in this paper. To explain the canopy collapse which happened in a powered parafoil test flight, the state parameters were solved at different thrust levels with the considering of the relative rotation between the canopy and the payload. The relationships between the configuration parameters and the thrust variable are discussed in this paper. A series of solutions for preventing canopy collapse are proposed.

II. Collapse Problem with Large Power

A powered seven-cell parafoil (Fig. 1) with a rectangular plane shape, a Clark-Y airfoil with 12% maximum thickness, a wingspan of 1.68 m, a chord length of 0.7 m, a leading-edge cut length of 0.07 m, a negative dihedral of 32.5 deg, and a canopy mass of 0.25 kg was studied. The payload under the canopy has a cylindrical shape and a propeller driven directly by an electronic motor; the payload has a mass of 1 kg and a maximum thrust of 10 N.

The parafoil was launched using manpower in test flights. It can be observed that, during several flights, the parafoil climbs steadily after takeoff with the appropriate power. The climbing angle increases with the increase of thrust until a critical value is reached, which causes the collapse of the canopy. Although the power is increased as slowly as possible, this collapse problem can still occur.

Because the phenomenon poses a critical threat to flight safety, analysis and proposals for improving the design are necessary.

a) b)

Fig. 1 Configuration of the parafoil discussed in this paper.

III. Static Model

Because the parafoil climbs in the longitudinal plane, it can be simplified to the model presented in Fig. 2, in which AB represents the section of the canopy, OA and OB represent the suspension lines, the origin O is the fixed point of the suspension lines on the payload, and C is the midpoint of the middle line in triangle ABO. All the lowercase letters represent the lengths or the angles.

The action point of the aerodynamic forces and the moments of the canopy are labeled point F, which is called the aerodynamic center. The centers of gravity of the canopy and payload are labeled O_1 and O_2. Assuming the action point of the aerodynamic drag of each suspension line, which are all supposed to have the same length, is its midpoint, the resultant drag of suspension lines acts on point C.

Because the change in the motor power is quite slow, the quasi-static assumption is valid here. Therefore, the system is assumed to be in an equilibrium state at all times. This situation requires solving four equations with four unknown values (α, γ, v, and δ) at equilibrium. To avoid the tension forces on suspension lines appear in the equations, two moments and two forces are given as follows:

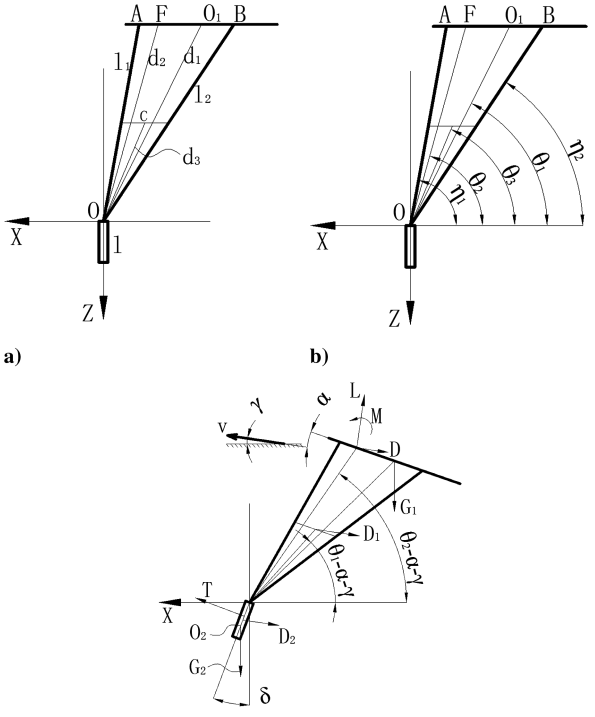

a) b) c)

Fig. 2 Simplified model of the parafoil.

$$\begin{cases} M_1 = M_0 - Ld_2\cos(\theta_2-\alpha) + Dd_2\sin(\theta_2-\alpha) \\ +G_1d_1\cos(\theta_1-\alpha-\gamma) + D_ld_3\sin(\theta_3-\alpha) \\ M_2 = Td_T - G_2d_G\sin\delta - D_2\frac{l}{2}\cos\gamma \\ F_X = T\cos\delta - L\sin\gamma - (D+D_l+D_2)\cos\gamma \\ F_Z = G_1+G_2-L\cos\gamma + (D+D_l+D_2)\sin\gamma - T\sin\delta \end{cases} \tag{1}$$

The equilibrium equations for the whole parafoil system in the longitudinal plane are given as follows: $M_1 = 0$, $M_2 = 0$, $F_X = 0$, $F_Z = 0$.

Because the parafoil just flies near the ground, the air density can be considered a constant. All of the aerodynamic forces and moments are only related to the angle of attack α and the speed v. Each given value of T has a corresponding flight state with certain values of α, γ, v, and δ.

The preceding equilibrium equations describe the necessary conditions for a steady flight. In addition, longitudinal static stability and tension in the suspension lines are also required for each steady flight.

A. Longitudinal Static Stability

The whole parafoil system should be able to restore itself after small disturbances. Because of the relative rotation between the canopy and the payload, the canopy-line combination and the payload should satisfy the following conditions separately:

$$\begin{cases} \frac{\partial M_1}{\partial\alpha} < 0 \\ \frac{\partial M_2}{\partial\delta} < 0 \end{cases} \tag{2}$$

B. Tension in the Suspension Lines

To avoid slack in the suspension line, the tension on the lines should be checked in each steady-flight state.

The force analysis on point O can be described as follows (Fig. 3): the force is pulling when positive.

$$\begin{cases} T_1\cos(\eta_1-\alpha-\gamma) + T_2\cos(\eta_2-\alpha-\gamma) = F_2\cos\eta \\ T_1\sin(\eta_1-\alpha-\gamma) + T_2\sin(\eta_2-\alpha-\gamma) = F_2\sin\eta \end{cases} \tag{3}$$

T_1 and T_2 are the corresponding tensions in the suspension lines, whereas F_2 equals to the resultant force on the payload, excluding the pulling force from the lines. The formulas of T_1 and T_2 are as follows:

$$\begin{cases} T_1 = F_2\frac{\sin(\eta_2-\alpha-\gamma-\eta)}{\sin(\eta_2-\eta_1)} \\ T_2 = F_2\frac{\sin(\eta_1-\alpha-\gamma-\eta)}{\sin(\eta_1-\eta_2)} \end{cases} \tag{4}$$

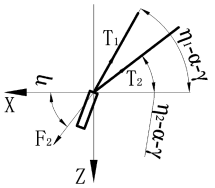

Fig. 3 Force analysis on point O.

Given $\eta_1 > \eta_2$, the following inequalities should be satisfied to ensure that the forces on the suspension lines are pulling forces:

$$\begin{cases} \eta - \eta_2 + \alpha + \gamma \geq 0 \\ \eta_1 - \alpha - \gamma - \eta \geq 0 \end{cases} \tag{5}$$

The physical meaning of the preceding inequalities is that the direction of F_2 should stay between the front and back lines.

C. Aerodynamic Forces and Moments

The lift coefficient and the induced drag coefficient are calculated by a program based on the vortex-lattice method (VLM). Compared with the engineering prediction, the VLM reflects the aerodynamic influence of the low aspect ratio and the high negative dihedral. Because of its assumption of steady, incompressible, inviscid, and irrotational flow, the VLM can only predict the lift and induced drag. However, as a quick and precise method in situations with a low angle of attack, the VLM is still more suitable than the engineering prediction for fast calculations of lift characteristics [16].

The following are the calculated aerodynamic coefficients correlated to lift for this parafoil: the lift coefficient is established as $C_L = 2.669\alpha + 0.1522$, in which α is the radian measured. The induced drag coefficient can be calculated as $C_{D_i} = 0.137C_L^2$. The zero-lift moment coefficient equals $C_{M_0} = -0.077$. In addition, the aerodynamic center is at 21.3% of the mean aerodynamic chord.

Other types of drag include the canopy zero-lift drag, line drag, and payload drag [13].

The drag coefficient for the open-airfoil nose is calculated as follows: $0.5h/c = 0.05$.

Summing up all items in Table 1 yields $C_{D_0} = 0.07$, and the action point is assumed to occur at the aerodynamic center of the canopy.

The line drag can be calculated as $C_{D_l} = (nRd_l/S)(\cos^3 \alpha_l)$.

It is assumed in the calculation that the lengths of the suspension lines are equal, the midpoint of the middle line of triangle ABO is the action point of the line drag, and $\alpha_l = \alpha + (\pi/2) - [(\theta_1 + \theta_2)/2)]$.

The payload drag is defined as $C_{D_s} = ld/S$, and the action point is at the midpoint of the payload.

All parameters which are needed by above estimations are listed in Table 2.

Table 1 Compositions of canopy zero-lift drag

Source of drag	Coefficient
Basic airfoil drag	0.015
Surface irregularities and fabric roughness	0.004
Open-airfoil nose	0.05
Drag of pennants and stabilizer panels	0.001

Table 2 Part of parameters for this parafoil

Symbol	Meanings	Values
n	Number of suspension lines	16
R	Mean line length (approximate to the average length of all suspension lines)	1.516 m
d_l	Suspension-line diameter	0.8 mm
S	Canopy area	1.1 m^2
θ_1	Marked in Fig. 2	75 deg
θ_2	Marked in Fig. 2	82.6 deg
l	Length of the payload	0.4 m
d	Payload diameter	0.1 m

IV. Results and Analysis

The equilibrium equations were solved by varying T from 0 to 10 N while considering the longitudinal static-stability condition and the tension condition in the suspension lines.

It can be observed from Figs. 4a–4e that when T increases, α, γ, v, and δ increase; v decreases; and the rate of v_z decreases. Figures 4f–4h show that the solved states have longitudinal static stability and that the suspension lines are tight. The parafoil can maintain a level flight only at one speed and one thrust. It is very different from a conventional airplane, which has many level-flight states. In addition, if an airplane maintains a level flight, the speed increases and the angle of attack decreases as a result of the increasing thrust. This behavior is different than that of a parafoil. The reason for the differences is mainly the lack of operating values for a powered parafoil.

If the thrust of the canopy is increased, the airfoil will consequently fall into a stall, which leads to collapse. Assuming the stalling incidence is 10 deg [10], the canopy collapse in test flights will occur when the value of T increases to 6.7 N.

Even if the maximum thrust of this parafoil is 10 N, it can only increase to 6.7 N in real flight because of its configuration parameters. There are two solutions to prevent this incompatibility between the configuration parameters and the motor thrust. One solution involves reducing the maximum thrust, and the other involves modifying the configuration parameters. The former will weaken the potential for a better performance, whereas the latter can access the potential at maximum thrust. Therefore, it is better to modify the configuration parameters to match the engine power.

V. Modification of the Configuration Parameters

The parafoil discussed previously cannot climb with a large amount of power at a large climbing angle. Therefore, it is necessary to study the relations between the configuration parameters and the flight performance to find a solution to this issue.

Without changing the aerodynamic characteristics of the parafoil, there are four modifiable configuration parameters: the position of the center of gravity of the payload, the length of the suspension lines, the deflection angle of the suspension lines, and the mass of the payload. To check the effect of any modifications, the following four performance parameters are defined:

1) The maximum available thrust $T_{\max}$ is the maximum required thrust for all steady flights before stalling. This value depends on the stalling incidence. The maximum power of the engine should not be greater than this value.

2) The maximum climbing rate $v_{z,\max}$ is the maximum climbing rate of all steady flights before stalling. This variable characterizes the climbing performance of a parafoil.

3) The required thrust for level flight T_{cruise} is the thrust value required to maintain the parafoil at a horizontal steady cruise. This variable characterizes the cruise performance of a parafoil.

4) The gliding angle γ_{glide} is the absolute value of the flight-path angle for steady gliding without power. The parameter has a negative correlation with gliding performance.

A. Changing the Center of Gravity of the Payload d_G

Because the length of the cylindrical payload is 0.4 m, α, γ, and v_z were calculated for the changing thrust, whereas d_G was varied from 0.16 to 0.36 m.

The method used to obtain the flight-performance parameters from Fig. 5 is as follows. If the maximum available thrust is smaller than 10 N, the value can be read from Fig. 5a while the vertical coordinate equals 10 deg, which is the stall angle of the canopy. The maximum climbing

Table 3 Units of different data lines in Fig. 10

Variable	Units
$T_{\max}$	N
$v_{z,\max}$	10 m/s
T_{cruise}	N
γ_{glide}	deg

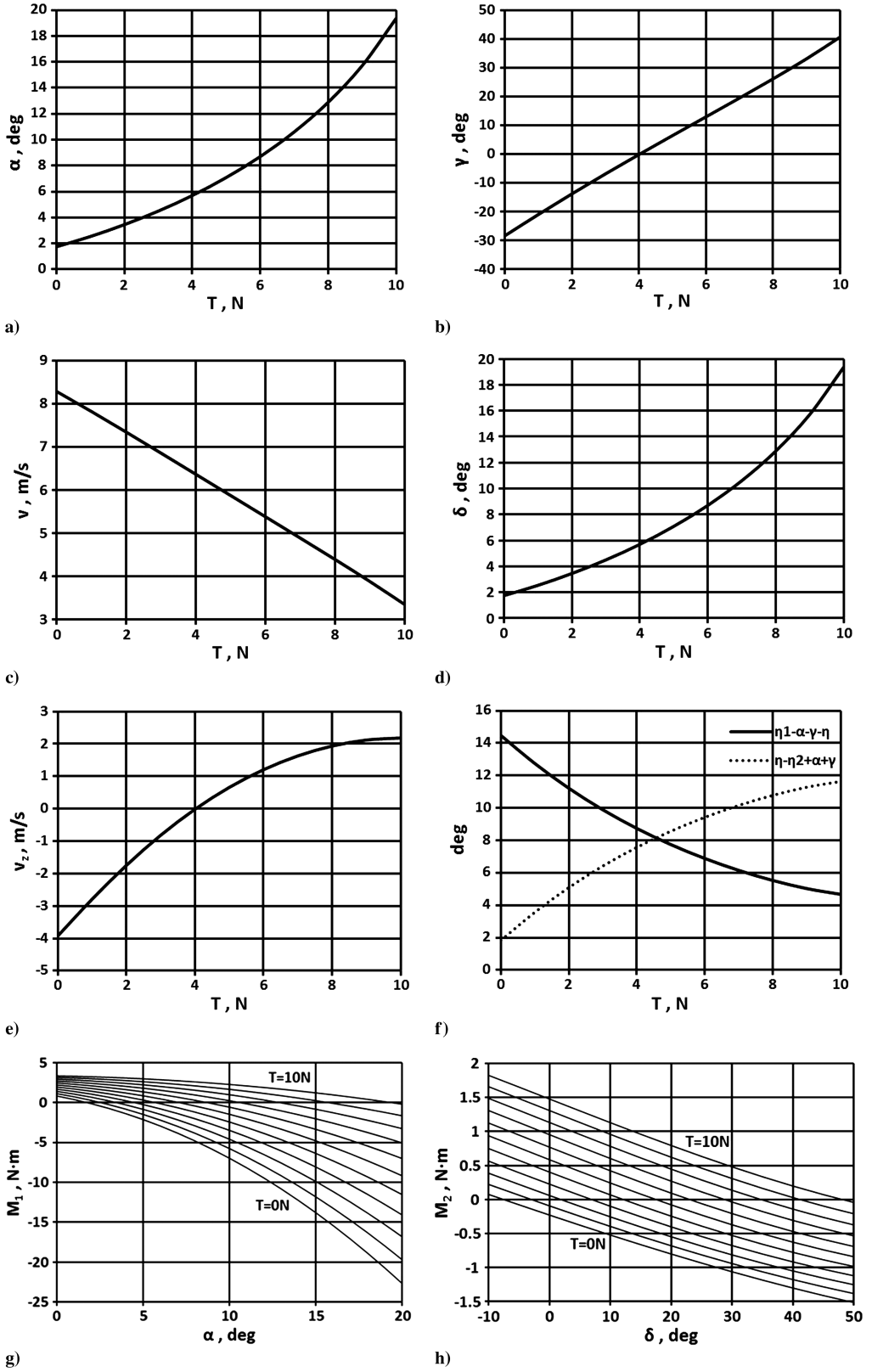

Fig. 4 Results of the equilibrium equations and the two checking conditions.

rate is obtained from the vertical coordinate, which corresponds to the maximum available thrust in Fig. 5b. The required thrust for level flight and the gliding angle can be read when the corresponding coordinates are 0 m/s in Fig. 5b and 0 N in Fig. 5c, respectively.

From these parameters, it can be observed that the maximum available thrust and the maximum climbing rate increase by increasing d_G, whereas the required thrust for level flight and the gliding angle change a little. It should be noted that static stability (2) and tension in the suspension lines (5) must always be satisfied.

B. Changing the Length of the Suspension Lines d_1

The variables α, γ, and v_z were calculated at various thrust levels, whereas d_1 was varied from 1.416 to 1.916 m.

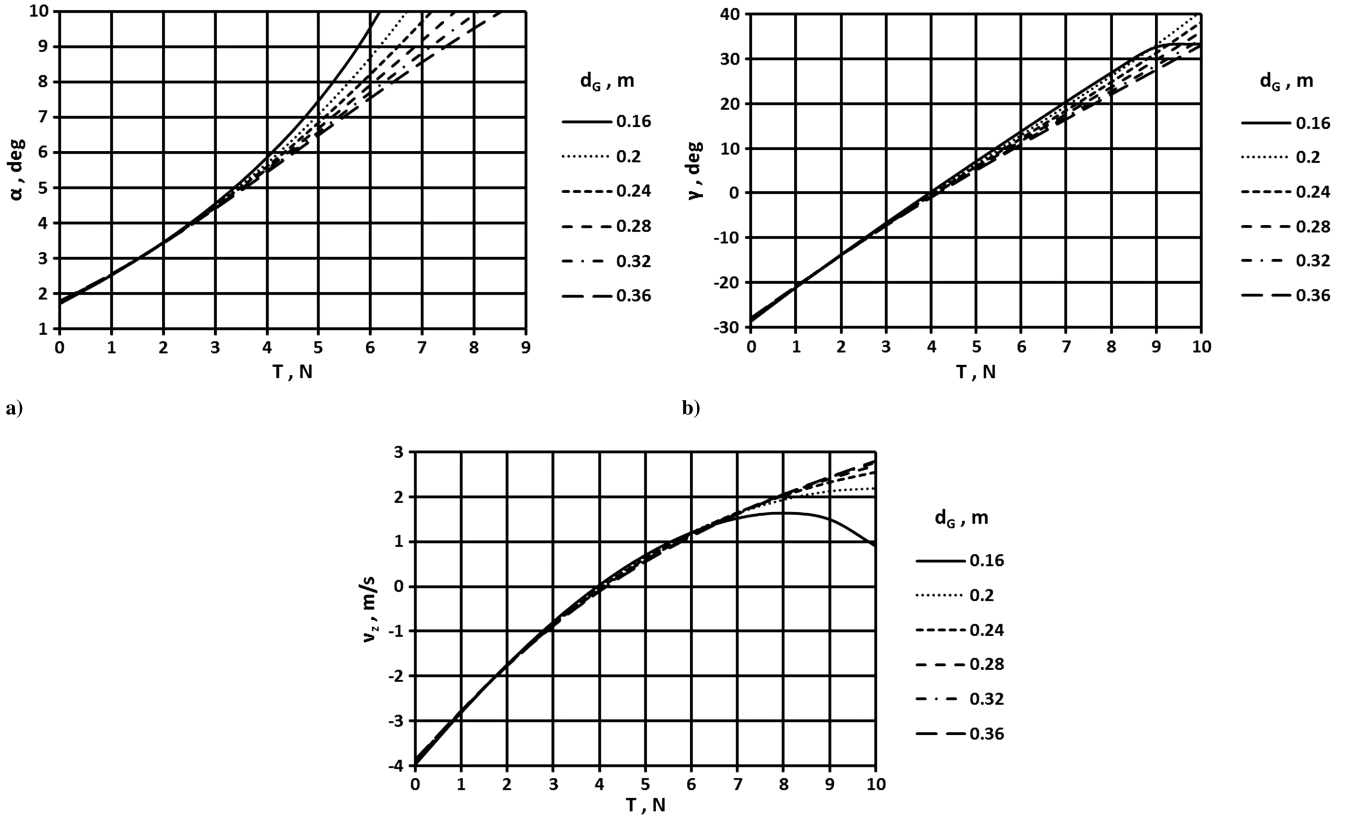

Fig. 5 Variation in the flight performance by changing d_G.

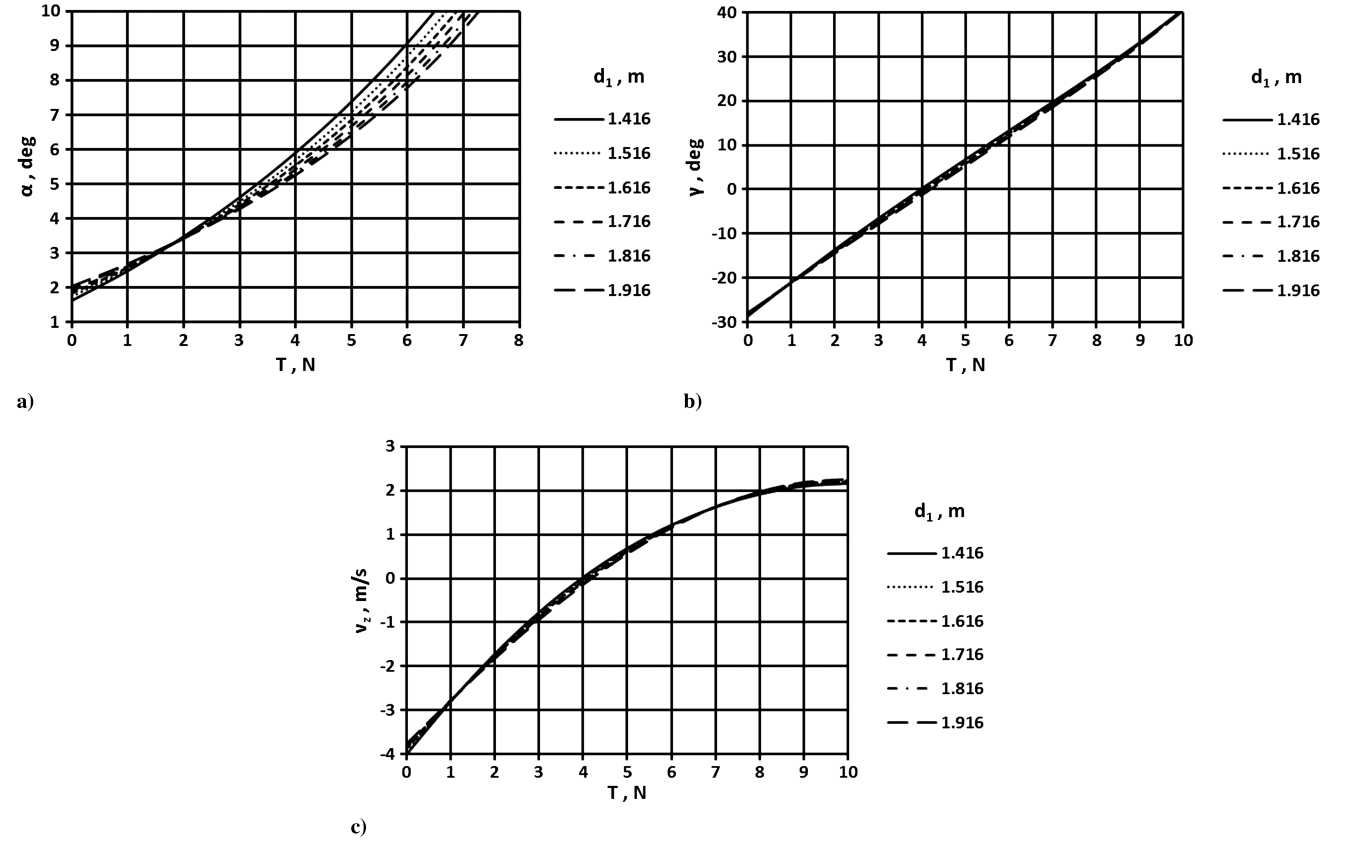

Fig. 6 Variation in the flight performance by changing d_1.

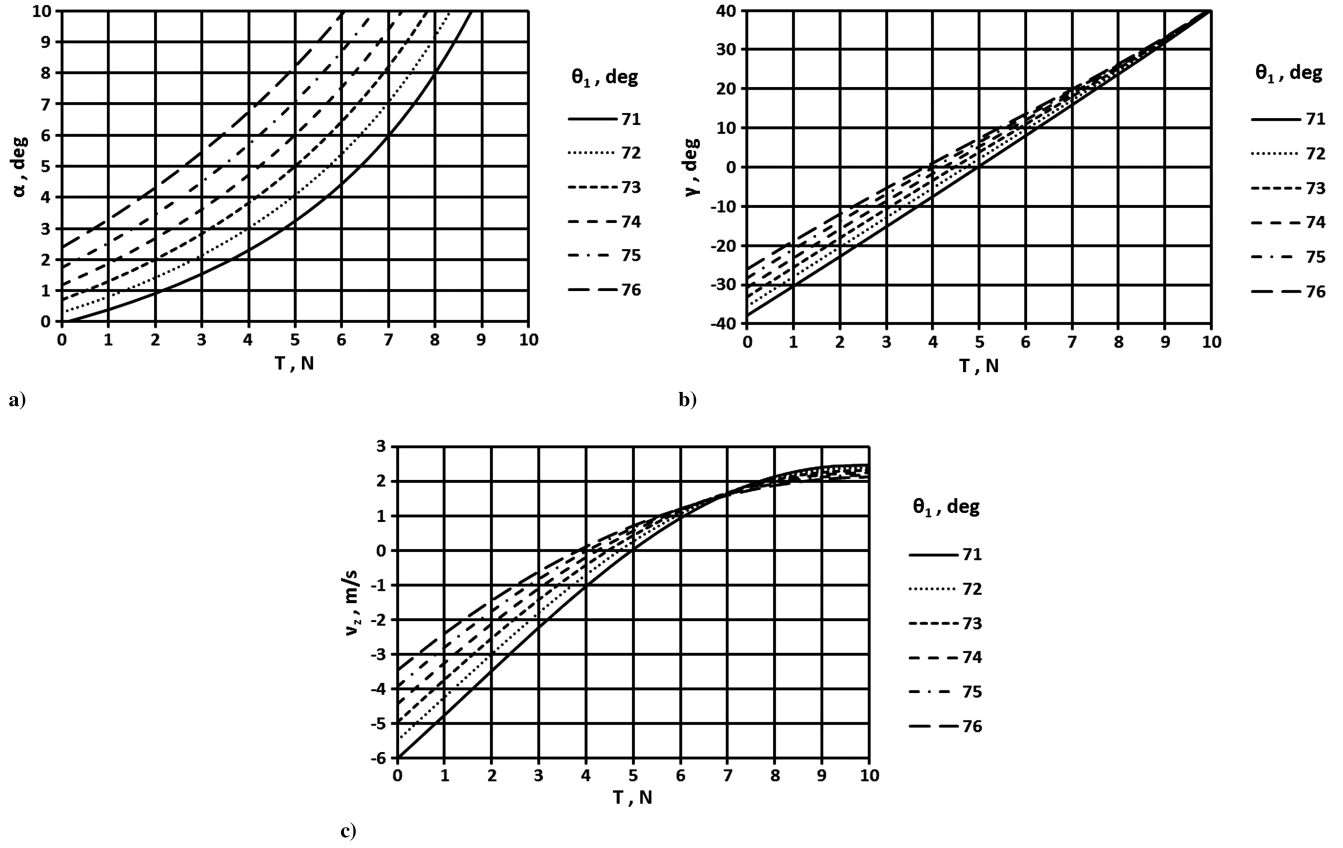

Fig. 7 Variation in the flight performance by changing θ_1.

As Fig. 6 shows, the maximum available thrust and the maximum climbing rate can be increased by increasing d_1. The required thrust for level flight and the gliding angle change a little, similar to Fig. 5. In addition, all of these states satisfy formulas (2) and (5).

C. Changing the Swing Angle of the Suspension Lines θ_1

The variables α, γ, and v_z were calculated at different thrust values, whereas θ_1 was varied from 71 to 76 deg.

As Fig. 7 shows, the maximum available thrust and the maximum climbing rate increase remarkably by increasing d_1, whereas the required thrust for level flight increases rapidly. Unfortunately, the gliding angle also increases.

After checking the tension force on the suspension lines, it was found that the result of the front line could be negative at small θ_1, as shown in Fig. 8. Specifically, if $\theta_1 < 73.8$ deg, the front suspension line will go slack when the motor has little power. In this situation, the parafoil could not fly steadily in some states. If the parafoil loses or decreases power in real flight, there would be a significant risk of collapse.

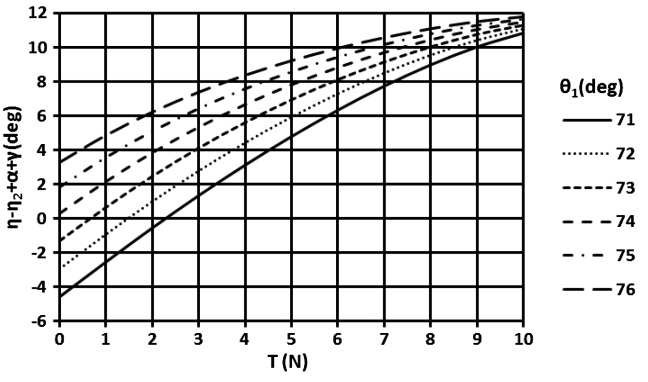

Fig. 8 Checking the tension condition for the front suspension line.

D. Changing the Mass of the Payload m_2

The variables α, γ, and v_z were calculated for varying levels of thrust, whereas m_2 was varied from 0.9 to 1.4 kg.

When d_1 increases in Fig. 9, the maximum available thrust increases sharply, which can ensure the parafoil maintains steady flight at the previous maximum thrust. The maximum climbing rate also increases remarkably by increasing d_1, whereas the required thrust for level flight increases dramatically and the gliding angle changes a little. In addition, formulas (2) and (5) are satisfied for all of these states.

E. Comparison

It should be noted that part of the data line for θ_1 in Fig. 10c does not have a physical meaning due to the slack in the front suspension line after $\theta_1 < 73.8$ deg.

To avoid the canopy-collapse problem studied in this paper, there are four improvements that can be made to enhance the performance at high power levels. The four improvements, which have a modification of increasing d_G, increasing d_1, decreasing θ_1, and increasing m_2, are marked plans 1–4. The maximum available thrust and climbing performance are all improved by the preceding methods. While plan 3 has the best climbing rate, it also has a strict requirement for swing angle. If the position of the payload surpasses the canopy too much, the parafoil would collapse under low thrust. Plan 4 demonstrates a considerable improvement in the climbing performance without the mentioned danger. However, it requires more power than the original plan for level cruise. Compared with plan 1, plan 2 shows less improvement in the climbing performance and a larger cruising thrust. To sum up, plan 1 not only has an acceptable cruising thrust that is close to the original value, but also an enhanced climbing performance. Furthermore, plan 1 involves minimum modifications to the original design.

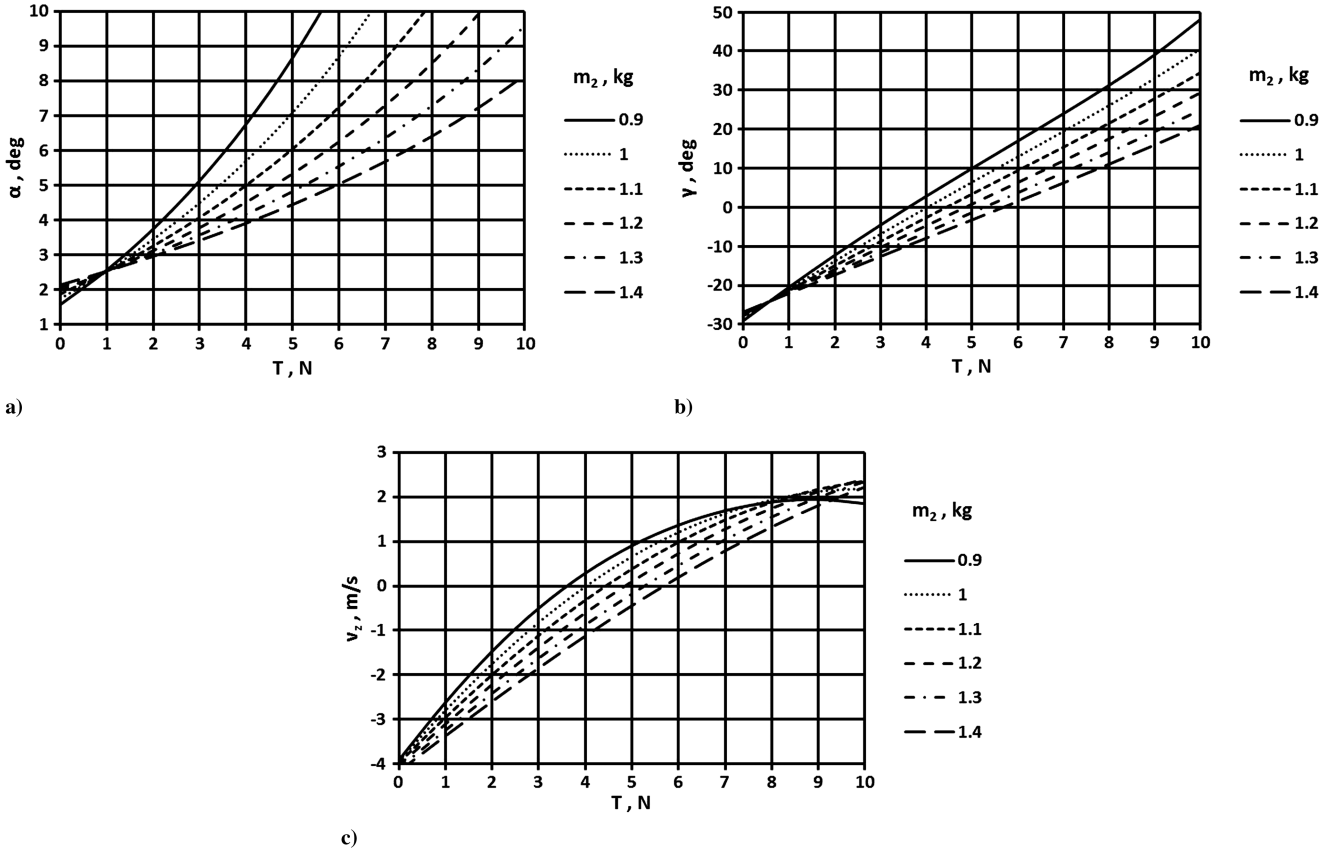

Fig. 9 Variation in the flight performance by changing m_2.

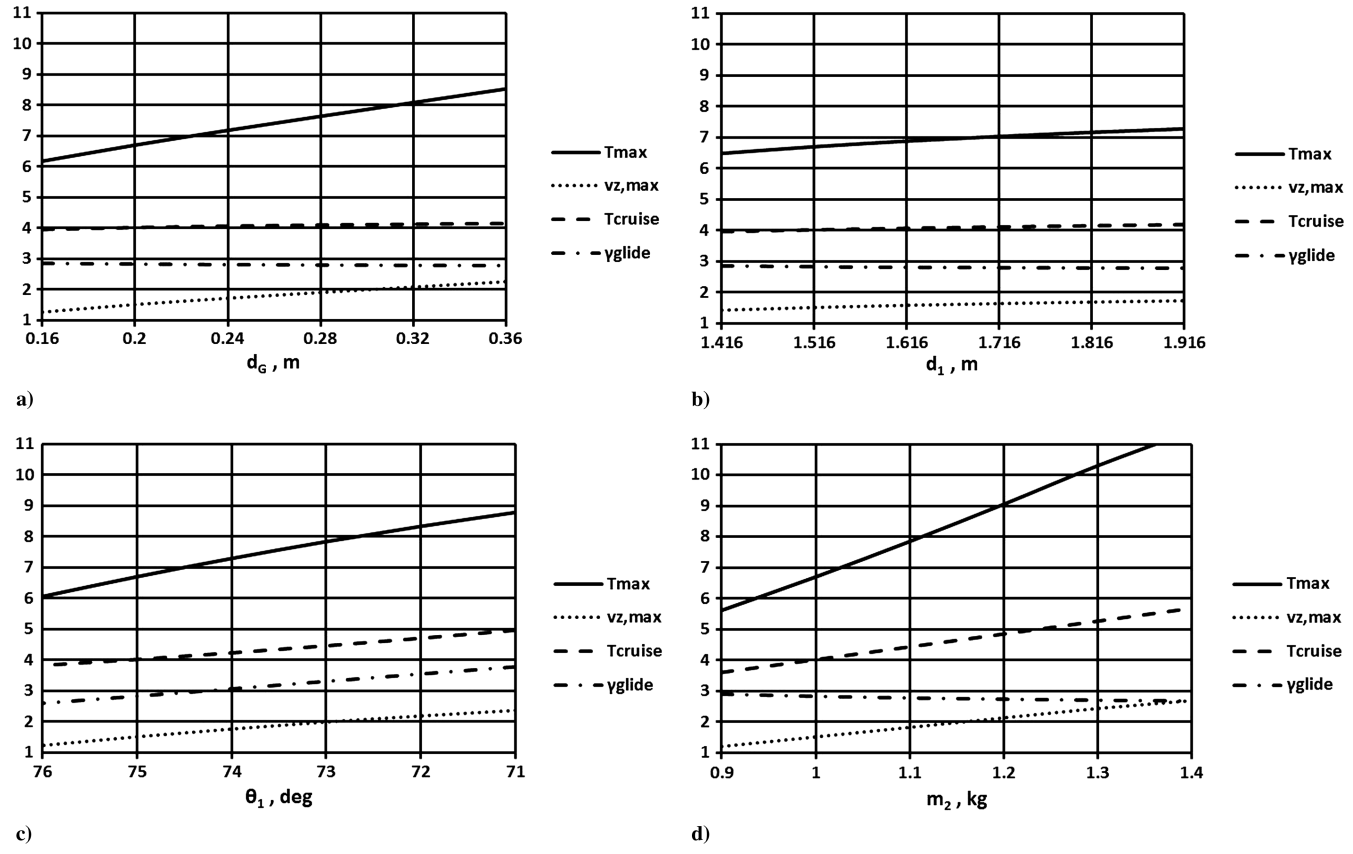

Fig. 10 Comparisons of the different methods for better performance.

The units of different data lines in Fig. 10 were listed in Table 3.

VI. Conclusions

The angle of attack of a powered parafoil increases by increasing the thrust. Because the stalling of the canopy must be avoided, a parafoil in flight has a maximum upper bound for the thrust variable. Furthermore, if the payload is located in the far front of the canopy, there will not only be an upper thrust limit, but also a lower one, which leads to the relaxation of the front suspension line. There are many ways to expand the range of available thrust and to achieve a better climbing performance. Lowering the center of gravity of the payload yields a better climbing rate without damaging the overall performance, and requires little modification of the original configuration.

In this paper, by considering the relative rotation between the payload and the canopy, a series of simple longitudinal static equations were established with checks of the longitudinal static stability and the tension in the suspension lines. This method can be used as a fast calculation of longitudinal flight performance for a parafoil with a similar configuration.

References

[1] Goodrick, T. F., "Theoretical Study of the Longitudinal Stability of High Performance Gliding Airdrop System," AIAA Paper 75-1394, Jan. 1963.

[2] Zhang, J., and Hou, Z., "Research on Longitudinal Dynamic Modeling of Powered Parafoil System," *Journal of System Simulation*, Vol. 22, No. 11, Nov. 2010, pp. 2541–2544 (in Chinese).

[3] Goodrick, T. F., "Simulation Studies of the Flight Dynamics of Gliding Parachute Systems," AIAA Paper 79-0417, Jan. 1963.

[4] Ge, Y., and Qin, Z., "Analyses of Glide and Stability Performance of Controllable Parafoil Systems," *Journal of National University of Defense Technology*, Vol. 14, No. 4, Nov. 1992, pp. 34–39 (in Chinese).

[5] Mortaloni, P., Yakimenko, O., Dobrokhodov, V., and Howard, R., "On the Development of a Six-Degree-of-Freedom Model of a Low-Aspect-Ratio Parafoil Delivery System," AIAA Paper 2003-2105, May 2003.

[6] Mooij, E., Wijnands, Q. G. J., and Schat, B., "9 DOF Parafoil/Payload Simulator Development and Validation," AIAA Paper 03-5459, Aug. 2003.

[7] Yakimenko, O., "On the Development of a Scalable 8-DoF Model of a Generic Parafoil-Based Delivery System," AIAA Paper 2005-1664, May 2005.

[8] Yakimenko, O., and Statnikov, R., "Multicriteria Parametrical Identification of the Parafoil-Load Delivery System," AIAA Paper 2005-1665, May 2005.

[9] Hiraki, K., "Experimental Approach to Identify the Longitudinal and Lateral Stability of Flexible Parafoil," AIAA Paper 2003-2145, May 2003.

[10] Nicolaides, J. D., "Parafoil Wind Tunnel Tests," AD731564, June 1971.

[11] Lingard, J. S., "The Aerodynamics of Gliding Parachutes," AIAA Paper 86-2427, Jan. 1963.

[12] Mohammadi, M. A., and Johari, H., "Computation of Flow over a High-Performance Parafoil Canopy," *Journal of Aircraft*, Vol. 47, No. 4, 2010, pp. 1338–1345.
doi:10.2514/1.47363

[13] Lingard, J. S., "Precision Aerial Delivery Seminar Ram-Air Parachute Design," *13th AIAA Aerodynamic Decelerator Systems Technology Conference*, Aerodynamic Decelerator Systems Technical Committee, May 1995.

[14] Redelinghuys, C., and Rhodes, S., "A Graphic Portrayal of Parafoil Trim and Static Stability," AIAA Paper 2007-2561, May 2007.

[15] Ward, M., Culpepper, S., and Costello, M., "Parametric Study of Powered Parafoil Flight Dynamics," AIAA Paper 2012-4726, Aug. 2012.

[16] Qian, Y., *Aerodynamics*, 5th ed., Beijing Univ. of Aeronautics and Astronautics Press, Beijing, 2005, pp. 153–169 (in Chinese).